# UNCERTAINTY QUANTIFICATION OF MATERIAL PROPERTIES IN BALLISTIC IMPACT OF MAGNESIUM ALLOYS

#### XINGSHENG SUN†

ABSTRACT. The design and development of cutting-edge light materials for extreme conditions including high-speed impact remains a continuing and significant challenge in spite of steady advances. Magnesium (Mg) and its alloys have gained much attention, due to their high strength-to-weight ratio and potential of further improvements in material properties such as strength and ductility. In this paper, we adopt a recently developed computational framework to quantify the effects of material uncertainties on the ballistic performance of Mg alloys. The framework is able to determine the largest deviation in the performance measure resulting from a finite variation in the corresponding material properties. It can also provide rigorous upper bounds on the probability of failure using known information about uncertainties and the system, and then conservative safety design and certification can be achieved. We specifically focus on AZ31B Mg alloys, and assume that the material is well-characterized by the Johnson-Cook constitutive and failure models, but the model parameters are uncertain. We determine the ordering of uncertainty contributions for model parameters and the corresponding behavior regimes where those parameters play a crucial role. Finally, we show that how this ordering provides insight on the improvement of ballistic performance and the development of new material models for Mg alloys.

Keywords. Uncertainty quantification; Ballistic impact; AZ31B magnesium alloys; Concentration of measure inequalities; Optimal uncertainty quantification

### 1. Introduction

The assessment and design of armor plates for protecting humans and vehicles against high-speed impact has long been of interest in military and aerospace applications. Among a large number of protection materials, magnesium (Mg) and its alloys have gained much attention, due to their high strength-to-weight ratio and potential of further improvements in material properties such as strength and ductility [1, 2, 3]. The density of Mg is approximately 35% lower than that of aluminum and approximately 77% lower than that of steel. Therefore, Mg alloys are the lightest metallic material that have high potential for weight reduction, thereby decreasing the amount of fuel used in military and aerospace applications [4, 5]. However, compared with other conventional materials, such as aluminum and steel, fewer studies have been performed on the relationship between material properties of Mg alloys and its ballistic response, particularly under extreme conditions, i.e., high strain-rates and temperatures [6, 7, 8].

The ballistic impact of materials and structures is characterized by a very complex mechanical-thermal coupled process which mainly depends on the material properties and geometrical parameters of the target and the projectile, e.g., strength, toughness, shape and size [9, 10, 11]. These extreme complexities, which involve high non-linearity, singularity and dependence on a large number of parameters, render it impossible to derive a closed-form analytical solution. As a result, numerical methods, e.g., finite element methods, have attracted more attention and been employed extensively in the modeling of ballistic impact

problems [12, 13, 14]. In the numerical modeling of ballistics, the responses of the materials to mechanical and thermal loading conditions are always described by constitutive and failure models, which supplies a stress-strain relation at multiple temperatures and strain rates in order to formulate governing equations along with the kinematic and conservation laws. These constitutive and failure models are usually *empirical*, representing the primary link between experimental inputs and predicted outputs and hence constituting the strongest source of physical fidelity in a given calculation. The data used to calibrate material models can be achieved either traditionally by laboratory experiments for simple specimens such as split Hopkinson bar [15, 16], or by sub-grid scale simulations such as crystal plasticity [17, 18]. Regardless of the source, analysts are most commonly restricted to a limited set of model forms, either by their simulation tool of choice or by the significant effort required to formulate, implement and characterize a new model. In practice, this restriction limits how well a fixed set of material parameters can fully represent a broad range of complex constitutive and failure behaviors. Therefore, the model parameters, characterizing multiple types of material properties, must be allowed to vary over a certain range, due to many factors including the potential complexity of response, any stochastic response characteristics, and the paucity of experimental data. These uncertainties render deterministic analysis of limited value. Instead, it becomes necessary to estimate the likely spread of performance metrics and relevant design requirement in order to provide an adequate design margin and meet specifications with sufficient confidence in the modeling of ballistic problems.

Within computational science, uncertainty quantification (UQ) is a family of powerful solution strategies that aim to characterize the variability of a given analysis and the spread in the predicted performance of a system [19, 20, 21, 22, 23]. The work presented in this paper focuses on systems in which the main source of uncertainty is an imperfect knowledge of material properties, as described by parameterized constitutive and failure models. The specific approach by which we quantify uncertainties is through the largest deviation in the performance measure resulting from a finite variation in the corresponding material properties, due to McDiarmid [24] belong to a general class known as concentration-ofmeasure (CoM) inequalities [25]. We also determine upper bounds of the probability that the system fails to perform within the design margin. Such bounds are rigorous, i.e., they are sure to be conservative and result in safe designs. These bounds are also optimal if we leverage all the known information about uncertainties and system using the optimal uncertainty quantification (OUQ) strategy [26]. This characterization of systems using CoM and OUQ requires only knowledge of limiting ranges of the input variables, and not their full probability distribution as is the case of Bayesian methods. The upper bound performance characteristics are computed by exercising an existing deterministic code in order to sample the mean response of the system and to calculate the largest deviation in output in order to identify worst-case combinations of parameters. The CoM and OUQ strategies have been used in various applications including design of a thermal-hydraulic reactor [27], design of a fractal electrical circuit [28], ballistic impact of aumnium alloys [29, 30, 31] and sub-ballistic impact of Mg alloys [32, 33].

The AZ31B type of Mg alloys is chosen in this study since AZ31B is widely used in aerospace and automotive applications [34, 35, 36, 37]. The goal of this work is to investigate how the uncertainties in the constitutive and failure properties of AZ31B affect its ballistic performance when the material is subject to high-speed impact, and then to provide insight on how to improve such performance and develop new material models for AZ31B.

For simplicity, we specifically hypothesize that the material behavior of AZ31B is known to be well-described by the Johnson-Cook constitutive and failure models [38, 39], but the corresponding material constants are only imperfectly characterized and within speficic ranges. Then, both the resulting uncertainty in the performance and the mean performance measure are computed using the DAKOTA Version 6.7 software package [40] of the Sandia National Laboratories. For all simulation parameters not considered as random variables, the values are considered as specified simulation conditions for evaluation. This strategy of fixing the boundary and initial conditions for assessment is entirely analogous to design testing for impact resistance [41], wherein performance is evaluated relative to a targeted set of precharacterized impact conditions. Simulations of such conditions are carried out over a range of impact velocities using the commercial finite-element package LS-DYNA [42] on a single converged mesh. The ballistic tests conform to the form of the Recht-Ipson model, and the material failure mechanisms for AZ31B are noteworthy including spalling, plugging, discing and fragmentation.

The remainder of the paper is structured as follows. In Section 2 we start by reviewing the CoM inequality, the OUQ approach and the corresponding probability bounds used for purposes of UQ. In Section 3, we proceed to investigate the effects of material uncertainties on the ballistic performance of AZ31B Mg alloys subject to high-speed impact. We conclude with a summary and short discussion in Section 4.

# 2. Methodology

For the sake of completeness and convenience, in this section we briefly summarize the CoM and OUQ theories for rigorous UQ and conservative safe design. Additional details can be found in Refs. [43, 26, 32].

2.1. Concentration-of-measure (CoM) inequality. We consider a system characterized by N real-valued random variables  $X \equiv (X_1, \ldots, X_N) \in \mathbb{R}^N$  and a single real-valued performance measure  $Y \in \mathbb{R}$ . The values of the input random variables lie within intervals  $I \equiv (I_1, \ldots, I_N)$ , i.e.,  $x_1 \in I_1, \ldots, x_N \in I_N$ . We begin by supposing that the system performance can be described by a deterministic response function  $F : \mathbb{R}^N \to \mathbb{R}$  through either experiments or an exact model. We further assume that the system fails if  $Y \geq Y_c$  where  $Y_c$  is a threshold value for the safe operation of the system, and that the expected system performance  $\mathbb{E}[Y]$  is known exactly. Then, a direct application of McDiarmid's concentration-of-measure (CoM) inequality [24] provides an upper bound on the probability-of-failure of the system [32]

(2.1) 
$$\mathbb{P}[Y \ge Y_c] \le \exp\left(-2\frac{\left(Y_c - \mathbb{E}[Y]\right)_+^2}{D^2}\right) \equiv P_{\mathrm{UB}},$$

where

(2.2) 
$$D = \left(\sum_{i=1}^{N} D_i^2\right)^{1/2}$$

is the system diameter and  $x_{+} := \max(x, 0)$ . In eq. (2.2),  $D_{i}$  denotes the sub-diameter corresponding to the input variable  $X_{i}$ , which is calculated through the optimization problem

(2.3) 
$$D_{i} = \sup_{\hat{x}_{i} \in \hat{I}_{i}, \ x_{i}, x'_{i} \in I_{i}} |F(\hat{x}_{i}, x_{i}) - F(\hat{x}_{i}, x'_{i})|,$$

where

$$\hat{x}_i = (x_1, \dots, x_{i-1}, x_{i+1}, \dots, x_N),$$

$$\hat{I}_i = I_1 \times \dots \times I_{i-1} \times I_{i+1} \times \dots \times I_N,$$

$$(2.4c) (\hat{x}_i, x_i) = (x_1, \dots, x_{i-1}, x_i, x_{i+1}, \dots, x_N),$$

(2.4d) 
$$(\hat{x}_i, x_i') = (x_1, \dots, x_{i-1}, x_i', x_{i+1}, \dots, x_N).$$

The preceding methodology can be extended to the case in which the exact mean performance  $\mathbb{E}[Y]$  is not available and the mean performance must be estimated instead. To this end, suppose that we conduct n evaluations of the model F(X) based on unbiased sampling of the random input variables, resulting in predicted performance measures  $y^1, y^2, \ldots, y^n$ . Then we can define an empirical mean performance as

(2.5) 
$$\langle Y \rangle = \frac{1}{n} \sum_{k=1}^{n} y^{k}.$$

Lucas et al. [43] showed that the probability of failure  $\mathbb{P}[Y \geq Y_c]$  can be determined to within confidence intervals by considering the randomness of the estimated mean  $\langle Y \rangle$ , with the result

(2.6) 
$$\mathbb{P}\left[\mathbb{P}[Y \ge Y_c] \ge \exp\left(-2\frac{\left(Y_c - \langle Y \rangle - \alpha\right)_+^2}{D^2}\right)\right] \le \epsilon',$$

where  $\epsilon'$  denotes a pre-specified tolerance for the mean estimation and D is the same as in eq. (2.2). In eq. (2.6),  $\alpha$  characterizes the effect of estimating mean performance, which has a form of

(2.7) 
$$\alpha = D\sqrt{\frac{-\ln \epsilon'}{2n}}.$$

Another equivalent expression of eq. (2.6) is that, with a probability that is greater than  $1 - \epsilon'$ , we have

(2.8) 
$$\mathbb{P}[Y \ge Y_c] \le \exp\left(-2\frac{\left(Y_c - \langle Y \rangle - \alpha\right)_+^2}{D^2}\right) \equiv P_{\text{UB}},$$

which also supplies an upper bound on the probability of failure for the scenario of estimating mean performance.

With these identifications, a conservative and rigorous design criterion can be achieved through requiring that this upper bound on the probability of failure less than a tolerance, with the result

(2.9) 
$$CF \equiv \frac{M}{U} \equiv \frac{(Y_c - \langle Y \rangle - \alpha)_+}{D} \ge \sqrt{\log \sqrt{\frac{1}{\epsilon}}},$$

where  $M = (Y_c - \langle Y \rangle - \alpha)_+$  measures the design margin and U = D provides an unambiguous definition and measure of uncertainty. The ratio CF of margin to uncertainty measures the confidence that can be placed on the design as is referred to as confidence factor. The design criterion eq. (2.9) simply requires that the confidence in the design, as measured by the confidence factor, be greater than a minimum value.

2.2. Optimal uncertainty quantification (OUQ). The McDiarmid's approach for UQ in eqs. (2.1) and (2.8) is attractive because it requires limited but tractable information on input variables (i.e., independence and intervals), response functions (i.e., sub-diameters) and performance measures (i.e., mean response). A question of theoretical and practical importance concerns whether it is possible to obtain an optimal bounds on the probability of failure using the same given information. Other related questions concerns the possibility of using other information than sub-diameters and mean output. These questions have been addressed by Owhadi et al. [26], and we proceed to summarize their main results for completeness. Assume that we want to certify the safety of a system and the criterion is given by

$$(2.10) \mathbb{P}[F(X) \ge Y_c] \le \epsilon$$

based on the information that  $X \equiv (X_1, \ldots, X_N)$ ,  $X_1, \ldots, X_N$  are independent,  $X \in I$  and that sup  $|F(\hat{x}_i, x_i) - F(\hat{x}_i, x_i')| \leq D_i$ ,  $\mathbb{E}[F] \leq 0$ . As a result, the optimal bound  $\mathcal{U}(\mathcal{A}_{MD})$  on the probability of failure  $\mathbb{P}[F(X) \geq Y_c]$  is the solution of the following optimization problem

(2.11) 
$$\mathcal{U}(\mathcal{A}_{MD}) = \sup_{(G,\mu)\in\mathcal{A}_{MD}} \mu[G(X) \ge Y_c]$$

where

(2.12) 
$$\mathcal{A}_{MD} = \left\{ (G, \mu) \middle| \begin{array}{l} G: I_1 \times \dots \times I_N \to \mathbb{R} \\ \mu \in \mathcal{M}(I_1) \otimes \dots \otimes \mathcal{M}(I_m) \\ \mathbb{E}_{\mu}[G] \leq 0 \\ \sup |G(\hat{x}_i, x_i) - G(\hat{x}_i, x_i')| \leq D_i \end{array} \right\}$$

and  $\mathcal{M}(I_i)$  denotes the set of probability measures on  $I_i$ .

In practical applications, the available information does not determine a unique solution of  $(G, \mathbb{P})$  but instead provides an information set  $\mathcal{A}$ . This set applies constraints on  $(G, \mathbb{P})$  and hence consists of all possible values of  $(G, \mathbb{P})$ . As a result, the optimal uncertainty quantification (OUQ) (Owhadi et al. [26]) aims to find the optimal bounds on probabilities given such set of information about the uncertainties. These bounds are calculated as extreme values of well-defined optimization problems corresponding to extremizing probabilities of deviation subject to the constraints imposed by the known information. As a result, McDiarmid's concentration-of-measure approach in eqs. (2.1) and (2.8) provides an upper bound on  $\mathcal{U}(\mathcal{A}_{MD})$ .

Although the optimization problem eq. (2.11) needs to be solved in infinite-dimensional spaces of measures and functions and therefore is extremely large, under general moment and independence conditions, Owhadi et al. [26] have shown that they have finite-dimensional reductions. An application of OUQ that is relevant to the present work concerns the development of explicit and optimal concentration inequalities of the McDiarmid's type. Namely, considering the information given in eq. (2.12) and assuming  $D_1 \geq \cdots \geq D_N$ , if  $Y_c \geq \sum_{i=1}^{N-2} D_i + D_N$ , the optimal bound is given by

$$(2.13) \qquad \mathcal{U}(\mathcal{A}_{MD}) = \begin{cases} 0 & \text{if } \sum_{i=1}^{N} D_{i} \leq Y_{c}, \\ \frac{(\sum_{i=1}^{N} D_{i} - Y_{c})^{N}}{N^{N} \prod_{i=1}^{N} D_{i}} & \text{if } \sum_{i=1}^{N} D_{i} - ND_{N} \leq Y_{c} \leq \sum_{i=1}^{N} D_{i}, \\ \frac{(\sum_{i=1}^{k} D_{i} - Y_{c})^{k}}{k^{k} \prod_{i=1}^{k} D_{i}} & \text{if, for } k \in \{1, ..., N-1\}, \\ \sum_{i=1}^{k} D_{i} - kD_{k} \leq Y_{c} \leq \sum_{j=1}^{k+1} D_{i} - (k+1)D_{k+1}. \end{cases}$$

We also refer to Owhadi et al. [26] for detailed derivation of eq. (2.13). The resultant optimal bounds provide a means of improving on the simple McDiarmid's bounds that are taken as the basis for the present work. Since the bounds are optimal, further improvements inevitably require information other than or in addition to system sub-diameters and mean performance.

# 3. Numerical experiments

We now proceed to quantify the uncertainties of the constitutive and failure properties in the modeling of a ballistic impact problem, using the UQ strategies described in the foregoing. Specifically, the target is an AZ31B Mg alloy plate and the projectile is a steel ball, as shown in Fig. 1(a). The residual velocity of the projectile is considered as the objective of interest in the numerical experiments, which can be considered as a metric to measure the performance of the plate subject to high-speed impact. Fig. 1(b) visualizes the system after penetration. We assume that all uncertainties arise from an imperfect characterization of the mechanical response of the plate. As a simple scenario, we further assume that, under the conditions of interest, the plate is well-characterized by the Johnson-Cook plasticity and fracture models [38, 39], but the parameters of the two models are uncertain. Specifically, they must be allowed to vary over certain ranges in order to cover the experimental data with prescribed probability. For simplicity, the projectile is assumed to be rigid and uncertainty-free.

3.1. Material modeling. We assume that the constitutive behavior of the plate is characterized by an appropriately calibrated Johnson-Cook plasticity model [38],

(3.1) 
$$\sigma(\epsilon_p, \dot{\epsilon}_p, T) = \left[A + B\epsilon_p^n\right] \left[1 + C \ln \dot{\epsilon}_p^*\right] \left[1 - T^{*m}\right],$$

where  $\sigma$  is the true Mises stress,  $\epsilon_p$  is the equivalent plastic strain,  $\dot{\epsilon}_p$  is the plastic strain rate, and T is the temperature. The normalized plastic strain rate  $\dot{\epsilon}_p^*$  is defined as

(3.2) 
$$\dot{\epsilon}_p^* := \frac{\dot{\epsilon}_p}{\dot{\epsilon}_{p0}},$$

where  $\dot{\epsilon}_{p0}$  is a reference strain rate. The model also uses the normalized temperature

(3.3) 
$$T^* := \frac{T - T_0}{T_m - T_0},$$

where  $T_0$  is a reference temperature and  $T_m$  is the melting temperature. The model parameters are: A, the yield stress; B, the strain-hardening modulus; n, the strain-hardening exponent; C, the strengthening coefficient of strain rate; and m, the thermal-softening exponent.

We further assume that the failure behavior of the plate is well-described by the Johnson-Cook fracture model [39]. Specifically, the damage of an element is defined on a cumulative damage parameter

$$(3.4) E = \sum \frac{\Delta \epsilon}{\epsilon f},$$

where the summation is conducted over time steps and  $\Delta \epsilon$  is the plastic strain increment in each time step.  $\epsilon^f$  denotes the strain at fracture which is given by

(3.5) 
$$\epsilon^f = \left[ E_1 + E_2 \exp(E_3 \sigma^*) \right] \left[ 1 + E_4 \ln \dot{\epsilon_p}^* \right] \left[ 1 + E_5 T^* \right],$$

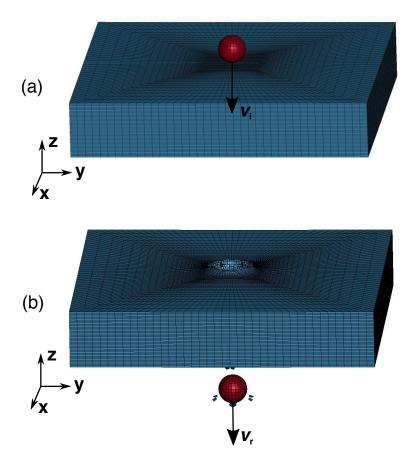


FIGURE 1. Schematic of the ballistic problem. (a) Initial setup of the projectile/plate system. (b) The system after perforation. The impact and the residual velocities of the projectile are denoted by  $v_i$  and  $v_r$ , respectively.

where  $E_1$ ,  $E_2$ ,  $E_3$ ,  $E_4$  and  $E_5$  are material damage constants.  $\epsilon_p^*$  and  $T^*$  are defined in eqs. 3.2 and 3.3, respectively.  $\sigma^*$  is the ratio of the pressure p divided by the von-Mises equivalent stress, i.e.,

(3.6) 
$$\sigma^* = \frac{p}{\sqrt{\frac{1}{2} \left[ (\sigma_1 - \sigma_2)^2 + (\sigma_2 - \sigma_3)^2 + (\sigma_3 - \sigma_1)^2 \right]}},$$

where  $\sigma_1$ ,  $\sigma_2$  and  $\sigma_3$  are the principle stresses. Based on this damage model, fracture takes place when the damage parameter E reaches the value of 1.

We regard the set  $X \equiv (A, B, n, C, m, E_1, E_2, E_3, E_4, E_5)$  of Johnson-Cook plasticity and damage parameters as the main source of uncertainty in the analysis. The estimated values and the bounds are tabulated in Table 1. In practice, the material parameters are derived from specific data sources, e.g., experiments or sub-grid simulations. We assume that these data are sufficient to determine confidence intervals for each parameter. In our calculations, we specifically use the AZ31B Mg alloy characterization of Hasenpouth [44], which, conveniently, includes the lower and upper bound of the 95% confidence intervals for Johnson-Cook plasticity parameters, i.e., A, B, n, C and m. In addition, regarding the Johnson-Cook damage parameters, the estimated values are provided by Feng et al. [45], but their bounds of confidence intervals are scarce in the literature. To this end, we add the

similar level of uncertainty, i.e., 10.0%, to the estimated values to generate the lower and upper bounds, and the resultant values are also shown in Table 1.

Table 1. Estimated values and bounds of AZ31B Johnson-Cook plasticity and damage parameters.

Parameter	Estimated value	Lower bound	Upper bound	Uncertainty
A  (MPa)	225.171	200.372	249.970	+/-11.01%
B  (MPa)	168.346	150.682	186.010	+/-10.49%
n	0.242	0.160	0.324	+/-33.88%
C	0.013	0.012	0.014	+/-7.69%
m	1.550	1.523	1.577	+/-1.74%
$E_1$	-0.35	-0.385	-0.315	+/-10.0%
$E_2$	0.6025	0.5423	0.6628	+/-10.0%
$E_3$	-0.4537	-0.4991	-0.4083	+/-10.0%
$E_4$	0.4738	0.4264	0.5212	+/-10.0%
$E_5$	7.2	6.48	7.92	+/-10.0%

Table 2. Fixed system parameters of the plate used in the ballistic problem.

Plate (AZ31B Mg)	Value	Unit	Source
Mass density	1.77	$\rm g/cm^3$	-
Young's modulus	45.0	GPa	-
Poisson's ratio	0.35	-	-
Specific heat	1.75	$J/(K \cdot g)$	[46]
Taylor-Quinney factor	0.6	-	[47]
Spall strength	1.5	GPa	[48]
Gruneisen intercept	4520.0	m/s	[49]
Gruneisen gamma	1.54	-	[49]
Gruneisen slope $S_1$	1.242	-	[49]
Reference strain rate	0.001	$s^{-1}$	[44]
Reference temperature	298.0	K	[44]
Reference melt. temp.	905.0	K	[44]
Plate length/width	5.08	$\mathrm{cm}$	-
Plate thickness	0.953	$\mathrm{cm}$	-

Table 3. Fixed system parameters of the projectile used in the ballistic problem.

Projectile (Steel)	Value	Unit
Mass density	7.83	$g/cm^3$
Young's modulus	210.0	GPa
Poisson's ratio	0.30	-
Diameter	0.476	$\mathrm{cm}$

3.2. Forward solver. For a given realization of the system parameters, the ballstic imapet problem is solved using the explicit dynamics solver available within the commercial finite element analysis software package LS-DYNA [42]. The initial conditions of the computational model are shown in Fig. 1(a). The plate is resolved using 185, 600 elements, while the number of elements for the projectile is 3,584. All the elements are linear hex, single point integration with careful hourglass control. Elements are refined in the impact region of the plate. This number and distribution of elements are enough to make the calculations converged. No constraint is applied on the plate. All simulations were ran for 30  $\mu$ s before termination. This simulation duration is sufficiently long to allow for either the penetration of the projectile through the plate, or the rebound and separation of the projectile from the plate. The timestep size is adaptive and determined by the critical size of elements. Element erosion is used to characterize material failure. Additionally, the calculations are adiabatic with the initial temperature set at room temperature. The equation-of-state, which controls the volumetric response of the material, is assumed to be of the Gruneisen type. The values of the fixed parameters of the plate and the projectile used in the calculations are tabulated in Tables 2 and 3, respectively.

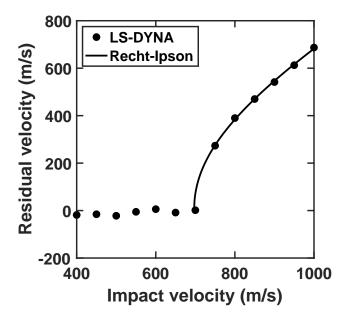


FIGURE 2. Residual velocity as a function of impact velocity.

3.3. Ballistic behavior. We begin by evaluating the ballistic property of the plate subject to normal impact, using one representative group of the Johnson-Cook plasticity and damage parameters listed in Table 1. Fig. 2 shows the residual velocity of the projectile, as a function of impact velocity ranging from 400 m/s to 1000 m/s. In order to estimate the ballistic limit, we employ the Recht-Ipson model [50], which provides an analytical expression based on the conversation of energy and momentum. Specifically, the model has the form of

(3.7) 
$$v_{\rm r} = a \left( v_{\rm i}^p - v_{\rm bl}^p \right)^{1/p},$$

where a, p and  $v_{bl}$  are fitting parameters. Specifically,  $v_{bl}$  represents the ballistic limit of the plate. The Recht-Ipson model is fitted to the residual perforation velocities calculated by

LS-DYNA, and the values of the fitting parameters are tabulated in Table 4. For comparison, the resulting Recht-Ipson curve is also plotted in Fig. 2. It is notable that the LS-DYNA results conform to the form of the Recht-Ipson model. The coefficient of determination  $R^2$  is extremely close to 1, also showing that the Recht-Ipson predictions well fit the LS-DYNA data. The predicted value of the ballistic limit by LS-DYNA calculations is 696.9 m/s. Moreover, although the parameter p is fitted to the numerical data, its value is very close to that given in the original Recht-Ipson model (i.e., p = 2).

Table 4. Values of Recht-Ipson parameters for the AZ31B Mg plate under consideration.

Parameter	$v_{\rm bl}~({\rm m/s})$	$\overline{a}$	p	$R^2$
Value	696.9	0.916	2.120	0.999

We proceed to examine material failure mechanisms involved in the LS-DYNA calculations. Fig. 3 shows the time history of the projectile velocity and the snapshots of the impact regions at three time instances of the calculation concerned with the normal strike with the impact velocity of 1000 m/s. Specifically, Fig. 3(b) shows level contours of maximum principal stress and temperature at the same moments in time. As may be seen from Fig. 3(a), the velocity of the projectile decreases smoothly during the penetration process. The penetration completes at around 20  $\mu$ s, and afterwards the velocity equals to a constant, i.e., the residual velocity. In addition, from Fig. 3(b) it is noteworthy that the LS-DYNA solver, when equipped with the element erosion criterion, is capable of capturing several well-known failure modes for materials under high-speed impact. Overall, the plate is perforated mainly by a conventional plugging mechanism. The impact energy is released by the large plastic work around the shear rupture that separates the cavity from the rest of the plate. The temperate field also peaks at the cavity boundary, resulting in thermal softening of the plate. This thermal softening in turn facilitates and promotes localization of deformation, eventually resulting in plugging formation. In addition to the shear plugging, spalling occurs in the region of high maximum principal stress near the backface of the plate at 2.8  $\mu$ s, due to the interaction between two reflecting tensile waves. Then at 11.2  $\mu$ s, because of the bending and stretching of the plate, several lateral cracks have appeared, which are parallel to the plane of the plate. As a result of the lateral cracks, discing happens near the backface of the plate at 30.0  $\mu$ s. The calculation also shows fragmented materials, which is typical for brittle materials such as AZ31B Mg alloys.

3.4. **UQ** analysis. Computing sub-diameters requires a constrained optimization over the space of input variables in order to determine the largest deviation in the performance measure. To this end, we employ a genetic algorithm (GA), which, as a global and derivative-free optimization method, provides the greatest flexibility in applications to non-linear problems. Another advantage of the GA is its high degree of concurrency. In particular, each iteration of the solution algorithm can be evaluated independently across multiple processors. In calculations, we employ the DAKOTA Version 6.7 software package [40] of the Sandia National Laboratories. We choose throughout a fixed population size of 64. One seed in the initial population is generated by setting the two repeated optimization variables associated with the sub-diameter at the two limits of that parameter range, with the remaining optimization variables set at the mid-span of their respective ranges. The remaining individuals in

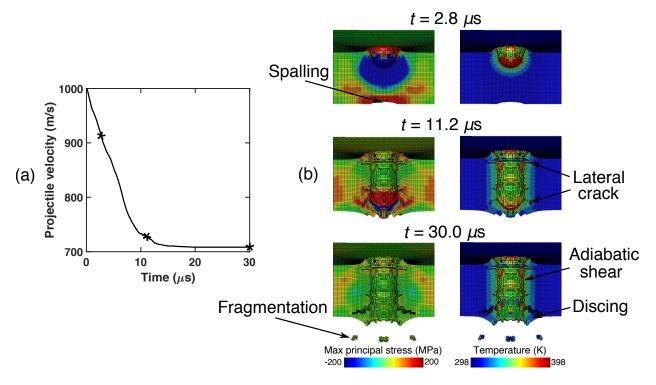


FIGURE 3. Normal impact of the AZ31B Mg plate with the initial velocity of 1000 m/s. (a) Time history of the projectile velocity. (b) Middle cross-section of the impact region. In Subfigure (a), the asterisks highlight the three time instances shown in Subfigure (b). In Subfigure (b), the projectile is removed for the sake of clarity.

the initial population are selected randomly. We find that this initial setup accelerates the convergence of the GA iterations. Additionally, the crossover and the mutation rates are 0.8 and 0.25, respectively. The numbers pf parents and offspring of each generation are 64 and 48, respectively. More details about the computational framework can be found at Ref. [32].

TABLE 5. Sub-diameters of Johnson-Cook parameters. The total diameter is 300.97 m/s, to which the plasticity and fracture models contribute 203.91 m/s and 221.37 m/s, respectively.

Johnson-Cook parameter	Sub-diameter (m/s)
$\overline{A}$	115.07
B	56.15
n	101.73
C	97.94
m	72.41
$E_1$	130.95
$E_2$	123.30
$E_3$	112.46
$E_4$	42.00
$E_5$	82.48

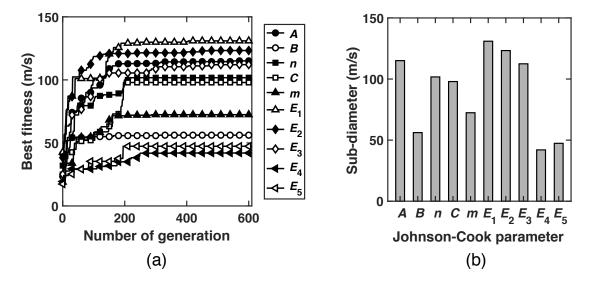


FIGURE 4. Uncertainty quantification for the ballistic problem. (a) History of the best fitness in GA calculations. (b) Sub-diameters of random parameters in Johnson-Cook plasticity and fracture models.

As aforementioned, the Johnson-Cook parameters A, B, n, C, m,  $E_1$ ,  $E_2$ ,  $E_3$ ,  $E_4$  and  $E_5$  are assumed to be uncertain and known to be within intervals only. Specifically, in the UQ analysis we investigate the worst-case scenario for all operating conditions under consideration, i.e., the largest velocity of 1000 m/s with normal impact. We use the residual velocity of the projectile as the performance measure of the system, which provides an excellent measurement for the behavior of the AZ31B Mg plate under high-speed impact. Fig. 4(a) shows the best fitness of each generation in the GA calculations. It is notable that, in spite of high non-linearity and irregularity of the fracture model and the contact condition used in the present ballistic problem, all GA calculations start to converge to a maxima after 200 to 300 generations. For the sake of comparison, Fig. 4(b) compares the sub-diameters computed for each of the material parameters of the Johnson-Cook plasticity and fracture models. The numerical values of the sub-diameters are also tabulated in Table 5. It is noteworthy that the sub-diameters are measured in the unit of the performance measure. Therefore, they all have the same unit. A direct consequence of this property is that the subdiameters can be compared and rank-ordered, which in turn provides a quantitative metric of the relative contributions of the parameters to the overall uncertainty of the response. From Fig. 4(b), we thus deduce this rank-ordering to be  $E_1 > E_2 > A > E_3 > n > C > m > B >$  $E_5 > E_4$ , with the parameters  $E_1$ ,  $E_2$  and A that contribute the most to the uncertainty, B,  $E_5$  and  $E_4$  the least and  $E_3$ , n, C and m intermediate. It is also notable that the contribution rank-ordering is different from the order of percentile variation of the random variables. For instance, compared to other parameters, the parameter n has the greatest percentile variation, cf. Table 1, but contributes only modestly to the total uncertainty in the system performance. This example evinces how relative uncertainties cannot be directly deduced from the variability of the input parameter in general, but also depend critically on the non-linear sensitivity of the system response to the parameters.

Another finding from the sub-diameters is the model-dependent analysis of uncertainty contributions. As mentioned before, we assume that the material uncertainty comes from

two separate models, i.e., Johnson-Cook plasticity and fracture models. Based on the subdiameters listed in Table 5, the corresponding total diameter is 300.97 m/s. The uncertainty contribution by the plasticity model, which includes the parameters A, B, n, C and m, is 203.91 m/s. By contrast, the fracture model, characterized by  $E_1$ ,  $E_2$ ,  $E_3$ ,  $E_4$  and  $E_5$ , contributes 221.37 m/s to the total uncertainty. Therefore, for the selected random parameters and their ranges under consideration, the Johnson-Cook fracture model contributes more to the uncertainty of the ballistic behavior of the AZ31B Mg alloy plate.

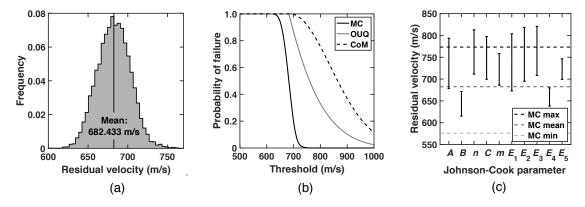


FIGURE 5. Comparison with MC sampling. (a) Histogram of output distribution by MC sampling. (b) Probability of failure computed from direct MC sampling and bounded by OUQ and CoM. (c) Residual velocities at the bounds of sub-diameters. In subfigure (c), the mean, maximum and minimum values of sampling results by MC are also shown.

As already mentioned, the present approach is predicated on probability inequalities as a means of bounding uncertainties. Evidently, the tighter the bound the better the design. However, increasing tightness comes at increasing computational expense, which sets forth a trade-off between economy of design and computability. Simple probability inequalities, such as McDiarmid's [24], supply a working compromise between tightness and computational complexity. However, it is both interesting and useful to investigate the tightness of the bounds and the attendant conservativeness of the designs. To this end, Fig. 5 shows comparisons between Monte Carlo (MC) sampling, concentration-of-measure (CoM) inequality and optimal uncertainty quantification (OUQ) for the projectile/plate system with impact velocity  $v_i = 1000 \text{ m/s}$  and normal attack. The MC sampling is performed over the ranges of the random parameters, using  $1.2 \times 10^4$  samples with Latin hypercube scheme and uniform distribution. Specifically, Fig. 5(a) shows the sampled distribution of the residual velocity Y. We compute  $\langle Y \rangle = 682.433$  m/s. Using this mean value, the upper bounds of the probability of failure through CoM and OUQ are shown in Fig. 5(b), compared with an estimate using the MC sampling. As expected, both the CoM and OUQ bounds lie uniformly above than the MC estimate, which illustrates the conservative character of the bounds and, by extension, of the corresponding designs. For the problem with the information of system sub-diameters and mean performance, OUQ provides the optimal bound. As a result, the OUQ bound is tighter than CoM bound, as also shown in Fig. 5(b). Moreover, Fig. 5(c) shows the two values of the residual velocity at the bounds of the sub-diameter for each random variable. The mean, maximum and minimum values of the sampled values of the residual velocity are also shown in Fig. 5(c). Notably, the residual velocities associated with the sub-diameters of A, n, C,  $E_1$ ,  $E_2$  and  $E_3$  are beyond the scope of MC data. These random parameters also contribute significantly to the total uncertainty in the performance of the plate. Thus, due to the sharp and irregular features involved in the contact and fracture problem, the random sampling method is not able to capture those extreme cases. By contrast, our UQ framework is capable of executing tests on demand over the entire operating space of random parameters, and hence provides required data for more rigorous uncertainty quantification and safer design.

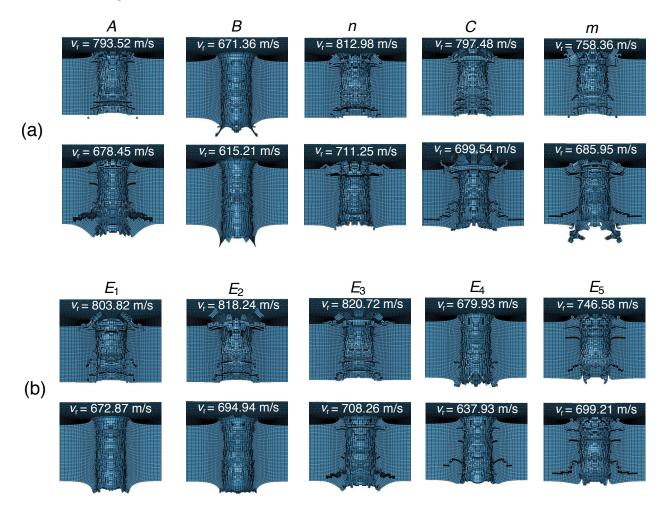


FIGURE 6. Snapshots of cavity after perforation at the bounds of sub-diameter for each random parameter. (a) Plasticity parameters. (b) Damage parameters.

The uncertainties considered in the present work come from the plasticity and fracture models, which characterize the strength and toughness of the materials, respectively. In order to explore the material regime in which the random parameters cause the largest deviation of the residual velocity, we extract the snapshots of the perforation cavity at the two bounds of the sub-diameter for each random variable, as shown in Fig. 6. Specifically, Fig. 6(a) and (b) visualize the profile of the cavity for the plasticity and fracture parameters, respectively. As may be seen from Fig. 6(a), the plasticity parameters result in the largest output uncertainty in different material regimes. Specifically, the behavior of the plate is more sensitive to the

parameters A, n, C and m when the plate is relatively brittle, whereas the parameter B has a significant effect in the regime of high toughness. Regarding the fracture parameters in Fig. 6(b), it is notable that the parameters  $E_1$ ,  $E_2$  and  $E_4$  have the largest uncertainty contribution in the range crossing both the ductile and brittle regimes. By contrast,  $E_3$  and  $E_5$  have a more significant contribution to the total uncertainty in the brittle regime.

## 4. Summary and concluding remarks

We have presented the implementation of a UQ framework to assess the effects of constitutive and fracture properties on the performance of Mg alloys subject to high speed impact. The quantification towards uncertainties is achieved by determining the largest deviation in the performance measure resulting from a finite variation in the corresponding input random variables. Both strategies of McDiarmid's CoM inequality and OUQ have been harnessed to calculate conservative upper bounds on the probability of failure, and then the safety of the system can be certified and designed rigorously using the QMU strategy. The McDiarmid's CoM inequality has a relatively simple formulation and hence can be easily employed, whereas the optimal UQ is able to provide the optimal bounds by leveraging all known information of uncertainties and measurements in spite of its complex equations. The uncertainties of the constitutive and fracture properties in the present work arise from the partial information of model parameters, determined either by experiments or by experience of experts.

Several significant findings afforded by the calculations are noteworthy. For our specific ballistic impact of AZ31B and the given intervals of uncertainties, the sub-diameters of the Johnson-Cook constitutive and fracture parameters are ordered as  $E_1 > E_2 > A > E_3 >$  $n > C > m > B > E_5 > E_4$ . Obviously, this ordering emphasizes the specific parameters where improvements are best targeted. Such a clear set of relationships also characterizes the constitutive and failure regime of interest, especially when compared against other boundary and/or initial conditions. For example, regarding the fracture models, the parameters related to the quasistatic behaviors, i.e.,  $E_1$ ,  $E_2$  and  $E_3$ , contribute more significantly to the ballistic performance of AZ31B compared to the strain-rate-related parameter  $E_4$  and temperaterelated parameter  $E_5$ . Therefore, the corresponding microscopic properties determining  $E_1$ ,  $E_2$  and  $E_3$  need to be adjusted in order to greatly improve the ballistic performance of the material. On the other hand, if a new fracture model needs to be developed for AZ31B, the part that affects its quasistatic behavior should gain more attention. Moreover, the material failure mechanisms for AZ31B involved in the impact tests bear emphasis, including spalling, plugging, discing and fragmentation, and our ballistic tests also conform to the form of the Recht-Ipson model.

We close with a comparison between the adopted UQ approach and Bayesian strategies. Bayesian inference, based on the Bayes' theorem, has been introduced as one of the main tools for UQ of the computational models, mainly due to the relative simplicity of implementation and the rigor of the resulting Bayesian analysis. Nevertheless, the quantification of uncertainties is conducted via calculating high-dimensional integrals that are very intractable or even impossible to evaluate analytically through conventional integration techniques, let alone those significantly complicated response functions that are achieved by existing open-source codes or commercial software. One numerical way to solve those integrals is Monte-Carlo sampling, which can become impractical if the probability of failure is small, i.e., if failure is a rare event, and if one-call of forward calculation is costly, as shown in the numerical

tests in this paper. By way of contrast, in the adopted method the response function can effectively be regarded as a black-box and the effort required for the computation of the uncertainty bounds only depends on the solution of sub-diameters and therefore is independent of the size of the probability of failure. In addition, the most commonly used priors in engineering problems are uniform and normal distributions. However, the strong influence of priors on the outcome of the inference process is also one of the most significant criticisms of Bayesian frameworks. By contrast, the CoM and OUQ approaches only requires the intervals of uncertain parameters and then provides rigorous bounds on the output uncertainties that bracket all the possible results led by all the probability measures in such intervals. If more information of uncertainties and system, such as moments of random variables, is given, the OUQ approach is able to obtain tighter bounds by leveraging such information.

#### ACKNOWLEDGMENTS

XS gratefully acknowledges the support of the University of Kentucky through the faculty startup fund.

## References

- [1] JT Lloyd, PA Jannotti, and TL Jones. An overview of penetration behavior in magnesium alloys. *Mechanics of Materials*, 162:104038, 2021.
- [2] Qiuming Wei, KT Ramesh, Todd C Hufnagel, Justin Wilkerson, Jaafar A El-Awady, Jamie Kimberley, Babak Ravaji, and Shailendra P Joshi. Insights from the mede program: An overview of microstructure–property linkages in the dynamic behaviors of magnesium alloys. *Mechanics of Materials*, 163:104084, 2021.
- [3] Suhas Eswarappa Prameela, Peng Yi, Yannick Hollenweger, Burigede Liu, Joey Chen, Laszlo Kecskes, Dennis M Kochmann, Michael L Falk, and Timothy P Weihs. Strengthening magnesium by design: Integrating alloying and dynamic processing. *Mechanics of Materials*, 167:104203, 2022.
- [4] M Dhari, M Autric, JE Masse, JF Mathieu, and G Barreau. Laser welding of az91 and we43 magnesium alloys for automotive and aerospace industries. *Advanced engineering materials*, 3, 2001.
- [5] Suveen N Mathaudhu and Eric A Nyberg. Magnesium alloys in us military applications: past, current and future solutions. *Essential readings in magnesium technology*, pages 71–76, 2016.
- [6] K Eswar Prasad, B Li, N Dixit, M Shaffer, SN Mathaudhu, and KT Ramesh. The dynamic flow and failure behavior of magnesium and magnesium alloys. *Jom*, 66(2):291–304, 2014.
- [7] Dingyi Sun, Mauricio Ponga, Kaushik Bhattacharya, and Michael Ortiz. Proliferation of twinning in hexagonal close-packed metals: application to magnesium. *Journal of the Mechanics and Physics of Solids*, 112:368–384, 2018.
- [8] Mauricio Ponga, Amuthan A Ramabathiran, Kaushik Bhattacharya, and Michael Ortiz. Dynamic behavior of nano-voids in magnesium under hydrostatic tensile stress. *Modelling and Simulation in Materials Science and Engineering*, 24(6):065003, 2016.
- [9] Iman Mohagheghian, GJ McShane, and WJ Stronge. Impact perforation of monolithic polyethylene plates: Projectile nose shape dependence. International Journal of impact engineering, 80:162–176, 2015.
- [10] PA Jannotti, NJ Lorenzo, TR Walter, BE Schuster, and JT Lloyd. Role of anisotropy in the ballistic response of rolled magnesium. *Mechanics of Materials*, 160:103953, 2021.
- [11] Jianfeng Liu, Yuan Long, Chong Ji, Qiang Liu, Mingshou Zhong, and Song Ge. Ballistic performance study on the composite structures of multi-layered targets subjected to high velocity impact by copper efp. Composite Structures, 184:484–496, 2018.
- [12] Liang Xue, Willis Mock Jr, and Ted Belytschko. Penetration of dh-36 steel plates with and without polyurea coating. *Mechanics of materials*, 42(11):981–1003, 2010.
- [13] B Li, A Kidane, G Ravichandran, and M Ortiz. Verification and validation of the optimal transportation meshfree (otm) simulation of terminal ballistics. *International Journal of Impact Engineering*, 42:25–36, 2012.

- [14] B Li, L Perotti, M Adams, J Mihaly, AJ Rosakis, M Stalzer, and Michael Ortiz. Large scale optimal transportation meshfree (otm) simulations of hypervelocity impact. *Procedia Engineering*, 58:320–327, 2013
- [15] I Ulacia, CP Salisbury, I Hurtado, and MJ Worswick. Tensile characterization and constitutive modeling of az31b magnesium alloy sheet over wide range of strain rates and temperatures. *Journal of Materials Processing Technology*, 211(5):830–839, 2011.
- [16] Dipankar Ghosh, Owen T Kingstedt, and Guruswami Ravichandran. Plastic work to heat conversion during high-strain rate deformation of mg and mg alloy. *Metallurgical and Materials Transactions A*, 48(1):14–19, 2017.
- [17] Jing Zhang and Shailendra P Joshi. Phenomenological crystal plasticity modeling and detailed micromechanical investigations of pure magnesium. *Journal of the Mechanics and Physics of Solids*, 60(5):945–972, 2012.
- [18] Yingrui Chang and Dennis M Kochmann. A variational constitutive model for slip-twinning interactions in hcp metals: application to single-and polycrystalline magnesium. *International Journal of Plasticity*, 73:39–61, 2015.
- [19] Nikola Kovachki, Burigede Liu, Xingsheng Sun, Hao Zhou, Kaushik Bhattacharya, Michael Ortiz, and Andrew Stuart. Multiscale modeling of materials: Computing, data science, uncertainty and goaloriented optimization. *Mechanics of Materials*, 165:104156, 2022.
- [20] Han Gao, Xueyu Zhu, and Jian-Xun Wang. A bi-fidelity surrogate modeling approach for uncertainty propagation in three-dimensional hemodynamic simulations. Computer Methods in Applied Mechanics and Engineering, 366:113047, 2020.
- [21] C Jiang, Z Zhang, X Han, and J Liu. A novel evidence-theory-based reliability analysis method for structures with epistemic uncertainty. *Computers & Structures*, 129:1–12, 2013.
- [22] Jie Liu, Xianghua Meng, Can Xu, Dequan Zhang, and Chao Jiang. Forward and inverse structural uncertainty propagations under stochastic variables with arbitrary probability distributions. *Computer Methods in Applied Mechanics and Engineering*, 342:287–320, 2018.
- [23] Jie Liu, Xingsheng Sun, Xu Han, Chao Jiang, and Dejie Yu. Dynamic load identification for stochastic structures based on gegenbauer polynomial approximation and regularization method. *Mechanical Systems and Signal Processing*, 56:35–54, 2015.
- [24] Colin McDiarmid. On the method of bounded differences. Surveys in combinatorics, 141(1):148–188, 1989.
- [25] M. Ledoux. The concentration of measure phenomenon. In *Mathematical Surveys and Monographs*, volume 89. American Mathematical Society, 2001.
- [26] H. Owhadi, C. Scovel, T. J. Sullivan, M. McKerns, and M. Ortiz. Optimal uncertainty quantification. SIAM Rev., 55(2):271–345, 2013.
- [27] Jerome Stenger, Fabrice Gamboa, Merlin Keller, and Bertrand Iooss. Optimal uncertainty quantification of a risk measurement from a thermal-hydraulic code using canonical moments. *International Journal for Uncertainty Quantification*, 10(1), 2020.
- [28] Ufuk Topcu, Leonard J Lucas, Houman Owhadi, and Michael Ortiz. Rigorous uncertainty quantification without integral testing. *Reliability Engineering & System Safety*, 96(9):1085–1091, 2011.
- [29] P-HT Kamga, B Li, M McKerns, LH Nguyen, M Ortiz, H Owhadi, and TJ Sullivan. Optimal uncertainty quantification with model uncertainty and legacy data. *Journal of the Mechanics and Physics of Solids*, 72:1–19, 2014.
- [30] A Kidane, A Lashgari, B Li, M McKerns, M Ortiz, H Owhadi, G Ravichandran, M Stalzer, and TJ Sullivan. Rigorous model-based uncertainty quantification with application to terminal ballistics, part i: Systems with controllable inputs and small scatter. *Journal of the Mechanics and Physics of Solids*, 60(5):983–1001, 2012.
- [31] M Adams, A Lashgari, B Li, M McKerns, J Mihaly, M Ortiz, H Owhadi, AJ Rosakis, M Stalzer, and TJ Sullivan. Rigorous model-based uncertainty quantification with application to terminal ballistics, part ii. systems with uncontrollable inputs and large scatter. *Journal of the Mechanics and Physics of Solids*, 60(5):1002–1019, 2012.
- [32] X Sun, T Kirchdoerfer, and M Ortiz. Rigorous uncertainty quantification and design with uncertain material models. *International Journal of Impact Engineering*, 136:103418, 2020.

- [33] Burigede Liu, Xingsheng Sun, Kaushik Bhattacharya, and Michael Ortiz. Hierarchical multiscale quantification of material uncertainty. *Journal of the Mechanics and Physics of Solids*, 153:104492, 2021.
- [34] Tyrone L Jones, Richard D DeLorme, Matthew S Burkins, and William A Gooch. Ballistic evaluation of magnesium alloy az31b. Technical report, Army Research Lab Aberdeen Proving Ground MD, 2007.
- [35] Juan Liu, Zhenshan Cui, and Congxing Li. Modelling of flow stress characterizing dynamic recrystallization for magnesium alloy az31b. *Computational Materials Science*, 41(3):375–382, 2008.
- [36] René Alderliesten, Calvin Rans, and Rinze Benedictus. The applicability of magnesium based fibre metal laminates in aerospace structures. *Composites Science and Technology*, 68(14):2983–2993, 2008.
- [37] Xingsheng Sun, Burigede Liu, Kaushik Bhattacharya, and Michael Ortiz. Concurrent goal-oriented materials-by-design. arXiv preprint arXiv:2106.06074, 2021.
- [38] Gordon R Johnson. A constitutive model and data for materials subjected to large strains, high strain rates, and high temperatures. *Proc. 7th Inf. Sympo. Ballistics*, pages 541–547, 1983.
- [39] Gordon R Johnson and William H Cook. Fracture characteristics of three metals subjected to various strains, strain rates, temperatures and pressures. *Engineering fracture mechanics*, 21(1):31–48, 1985.
- [40] Brian M Adams, L.E. Bauman, W.J. Bohnhoff, K.R. Dalbey, M.S. Ebeida, J.P. Eddy, M.S. Eldred, P.D. Hough, K.T. Hu, J.D. Jakeman, J.A. Stephens, L.P. Swiler, D.M. Vigil, and T.M. Wildey. Dakota, a multilevel parallel object-oriented framework for design optimization, parameter estimation, uncertainty quantification, and sensitivity analysis: version 6.7 user's manual. Sandia National Laboratories, Tech. Rep. SAND2014-4253, 2014.
- [41] MB Mukasey, Jeffrey L Sedgwick, and DW Hagy. Ballistic resistance of body armor, nij standard-0101.06. US Department of Justice (www. ojp. usdoj. gov/nij), 2008.
- [42] John O Hallquist et al. Ls-dyna keyword user's manual. Livermore Software Technology Corporation, 970:299–800, 2007.
- [43] Leonard J Lucas, H Owhadi, and M Ortiz. Rigorous verification, validation, uncertainty quantification and certification through concentration-of-measure inequalities. Computer Methods in Applied Mechanics and Engineering, 197(51-52):4591-4609, 2008.
- [44] Dan Hasenpouth. Tensile high strain rate behavior of az31b magnesium alloy sheet. Master's thesis, University of Waterloo, 2010.
- [45] Fei Feng, Shangyu Huang, Zhenghua Meng, Jianhua Hu, Yu Lei, Mengcheng Zhou, and Zhenzhen Yang. A constitutive and fracture model for az31b magnesium alloy in the tensile state. *Materials Science and Engineering:* A, 594:334–343, 2014.
- [46] Sanghyun Lee, Hye Jeong Ham, Su Yong Kwon, Sok Won Kim, and Chang Min Suh. Thermal conductivity of magnesium alloys in the temperature range from 125 c to 400 c. *International Journal of Thermophysics*, 34:2343–2350, 2013.
- [47] Owen T Kingstedt and Jeffrey T Lloyd. On the conversion of plastic work to heat in mg alloy az31b for dislocation slip and twinning deformation. *Mechanics of Materials*, 134:176–184, 2019.
- [48] L Farbaniec, CL Williams, L Kecskes, KT Ramesh, and R Becker. Microstructural effects on the spall properties of ECAE-processed AZ31B magnesium alloy. *International Journal of Impact Engineering*, 98:34–41, 2016.
- [49] J Feng, P Chen, Q Zhou, K Dai, E An, and Y Yuan. Numerical simulation of explosive welding using smoothed particle hydrodynamics method. *International Journal of Multiphysics*, 11, 2017.
- [50] RF Recht and TW Ipson. Ballistic perforation dynamics. Journal of Applied Mechanics, 30(3):384–390, 1963.

Department of Mechanical and Aerospace Engineering, University of Kentucky, Lexington, KY 40506, USA. † Corresponding author. E-mail address: xingsheng.sun@uky.edu.